Study of interface phenomena between bone and titanium and alumina surfaces in the case of monolithic and composite dental implants

D. KORN, G. SOYEZ, G. ELSSNER, G. PETZOW
Max-Planck-Institut für Metallforschung, Seestraße 92, 70174 Stuttgart, Germany

E. F. BRÈS
Laboratoire de Métallurgie Physique, LSPES URA CNRS 234, Université de Lille 1, Bâtiment C6, 59655 Villeneuve d'Ascq cedex, France

B. d'HOEDT, W. SCHULTE
Sonderforschungsbereich 175, "Implantologie", Calwerstraße, 7/7, 72076 Tübingen, Germany

The interface between mandibular bone and dental implants was examined with the *in vivo* dog model. Implant/bone interfaces were investigated for three types of materials: Ti–30 wt % Ta/Al_2O_3, titanium and Al_2O_3 using microscopy techniques covering a large magnification range: scanning electron microscopy, transmission electron microscopy, energy dispersive X-ray analysis and Auger spectroscopy. During the interaction of the Al_2O_3 ceramic with bone, an interfacial layer about 15 μm thick is formed. The same phenomenon was observed at the titanium bone interface, where the thickness of the layer was about 10 μm. In all cases, interface layers were sharp with well-defined borders between bone tissue and implant materials. No calcification took place inside the interface layer. A chemical analysis performed on this layer shows the presence of titanium, calcium and phosphorus in the case of titanium implants, and aluminium, calcium and phosphorus in the case of alumina implants. A rapid decrease in metal composition with increasing distances from the implant surface is correlated to a slow increase in calcium and phosphorus in the direction of the bone. Direct contact between implant and bone was observed. No biocorrosive effects were detected at the Ti–30 wt % Ta/Al_2O_3 metal–ceramic interface.

1. Introduction

The replacement of teeth of increasingly younger patients, for example in the case of trauma, requires the design of dental implants with a stability maintained over several decades. Such implant systems must permit the transfer of load and avoid any negative local or systematic tissue effects during the lifetime of the patient [1–3]. For such properties to be fulfilled, the interactive events taking place at the interface between the implant and the recipient tissue must be well understood.

In the present study, the interface between bone and three types of materials has been studied: Al_2O_3, titanium and Ti–30 wt % Ta/Al_2O_3. All materials used are corrosion-resistant to physiological solutions [4, 5].

The Ti–30 wt % Ta/Al_2O_3 implants were fabricated at the Max-Planck Institute of Stuttgart in collaboration with dental surgeons of the University of Tübingen [6]. They were tested *in vivo* in order to investigate the implant/bone interface [7, 8] and their biocompatibility [9].

Several microscopical and analytical techniques, scanning electron microscopy (SEM), transmission electron microscopy (TEM), microprobe measurements with energy dispersive spectroscopy (EDS) and Auger electron spectroscopy (AES) were used. Information was obtained at a large range of magnifications concerning both the structural events and the chemical interactions taking place at the interface between the implant material and bone.

2. Materials and methods

2.1. Materials

Commercially pure titanium (99.6%), pure alumina (99.7%) with a grain size of about 10 μm and a porosity of less than 1%, and diffusion-bonded Ti–30 wt % Ta/Al_2O_3 have been used. Alumina was sintered with MgO additive. The manufacturing of the

0957–4530

TABLE I Implant materials and conditions of implantation

Type of implant	Material	Duration of implantation (months)	Bone contact (%)
Cylinder	Ti–30 wt % Ta/Al_2O_3	5	25–33
Cylinder	Commercially pure Ti	5	25–33
Cylinder	Al_2O_3	5	43

metal–ceramic composites and their structure and mechanical properties are described elsewhere [6, 10]. The implants have a cylindrical shape with both diameter and length of 5 mm.

2.2. Surgical procedure and specimen preparation

The cylindrical devices were fully implanted into the mandibular bone of foxhounds for a period of 5 months without any functional loading (Table I). The animal euthanasia and implantation control were carried out at the University of Heidelberg [7].

The devices were explanted after 5 months with their surrounding bone tissue then fixed, dehydrated and embedded in epoxy duroplast in order to form a block which was subsequently ground in three steps using SiC papers down to grit size 1200 [11, 12]. Histological and histomorphological studies were first performed by light microscopy in order to evaluate the contact area between implant and bone [13, 14] (Table I) before examination by SEM, TEM, EDS and AES.

Cross-sections of the samples for EDS and SEM studies were been cut with a diamond saw. Carbon was sputtered on the samples for electrical conduction.

Samples for TEM were prepared by a technique specially developed for preparing brittle materials and weakly bonded interfaces [15]. Slices of about 300 μm were cut parallel to the interface and fitted into a slit in an alumina cylinder. This arrangement was inserted inside a second, hollow, 3 mm diameter alumina cylinder, and further embedded in epoxy resin. After complete hardening, slices of about 500 μm were cut perpendicular to the interface and therefore perpendicular to the axis of the alumina cylinder by using a diamond saw. Planparallel specimens of 100–200 μm were obtained by grinding. Subsequently, the samples were dimpled in order to obtain a residual thickness in the centre of the specimen between 10 and 50 μm. In the last preparation step, the centre of the samples was thinned by ion milling in order to obtain non-decalcified electron-transparent interfaces.

2.3. Microscopic and analytical techniques

The SEM analysis of the samples was carried out on a Jeol JSM 35 microscope equipped with a Tracor Northern TN 2000 electron dispersion spectrometer (EDS) and on a Jeol JSM 6400 microscope.

TEM experiments were performed on a Jeol 2000FX TEM microscope. The EDS analysis was made with an Explorer Noran Ge detector.

The Auger electron spectroscopy analysis was carried out with a Perkin–Elmer SAM 500. The angle between the surface normal and the analysor axis was 30°. The primary electrons had an energy of 10 keV. The spectra to be interpreted were the differential of the energy of the monitored Auger intensities. The surface composition was directly correlated to the peak-to-peak heights of the differentiated Auger intensities [16].

3. Results

3.1. Ti–30 wt% Ta/Al_2O_3/bone interface

The Ti–30 wt % Ta/bone, Al_2O_3/bone interfaces and the Ti–30 wt % Ta/Al_2O_3/bone triple points were examined using SEM. Three different interface morphologies were observed: (i) a direct contact; (ii) an intermediate layer; (iii) a gap at the implant/bone interface. A direct contact with bone is observed at the region where Ti–30 wt % Ta and Al_2O_3 are fitted (Fig. 1). The micrograph shows that the metal–ceramic interface does not impair the contact between implant and bone. The bone exactly accommodates to the composite implant surface especially at step **S**. Additionally, parallel (**C**) and ellipsoidal features (**OC**) can be observed independently to the adjacent implant region.

These parallel (**C**) and ellipsoidal (**OC**) features of bone were also detected at the Ti–30 wt % Ta side of the implant (Fig. 2). The dark interlayer, **DI** (Fig. 3), is adjacent to the Al_2O_3 part of the implant and can also be observed at other interface situations. It attains thicknesses up to 50 μm at the Al_2O_3/bone interface (Fig. 3). On the right hand side of Fig. 3, a gap, **G**, is observed at the alumina/bone interface. This seems to

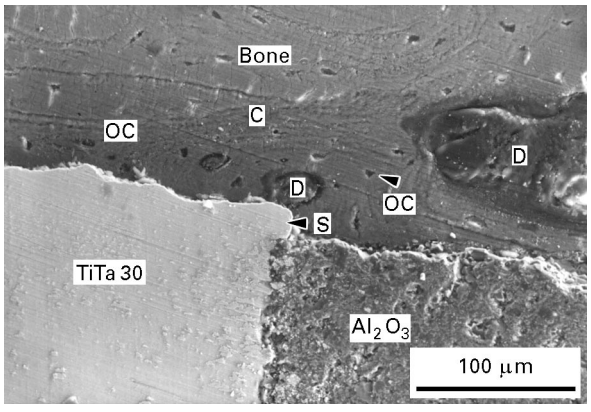

Figure 1 The interface between Ti–30 wt % Ta/alumina and bone. **OC**, osteocytes; **C**, collagen; **D**, undefined dark region; **S**, step.

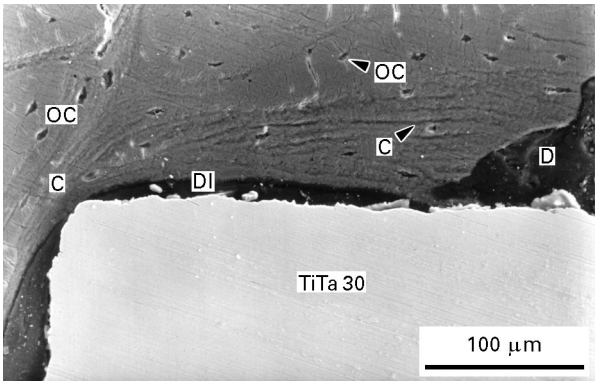

Figure 2 Ti–30 wt% Ta/bone interface of the Ti–30 wt% Ta/Al_2O_3 implant separated by an intermediate layer of 100 μm maximum thickness mainly consisting of carbon. **OC**, osteocytes; **C**, collagen; **DI**, dark interlayer.

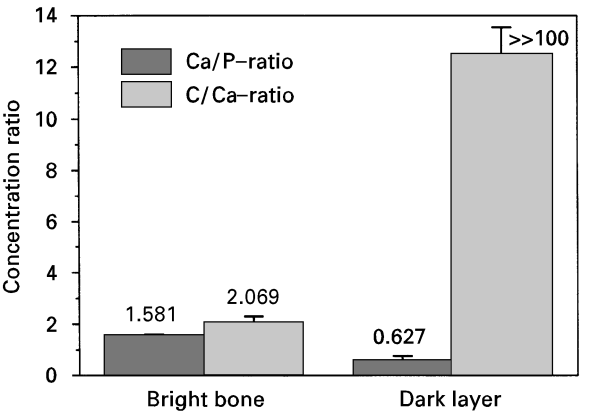

Figure 4 Microprobe analysis of the bright bone region and the dark interlayer in EDS mode.

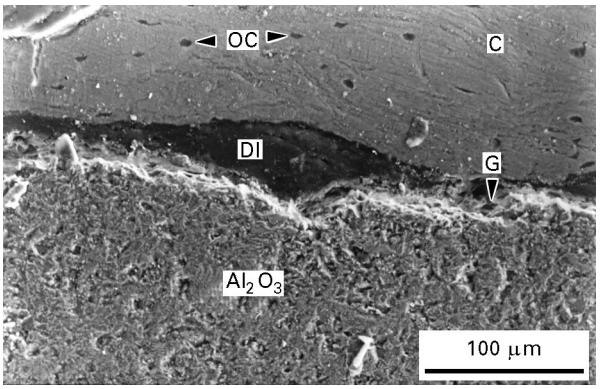

Figure 3 Al_2O_3/bone interface of the Ti–30 wt% Ta/Al_2O_3 implant interrupted by an intermediate layer of 50 μm maximum thickness mainly consisting of carbon. **OC**, osteocytes; **C**, collagen; **G**, interface gap.

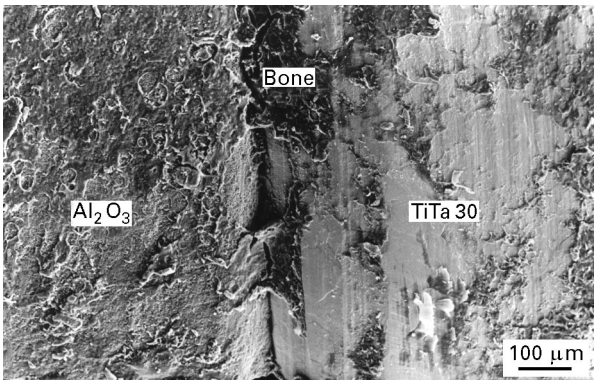

Figure 5 Fracture surface of the Ti–30 wt% Ta/Al_2O_3 implant.

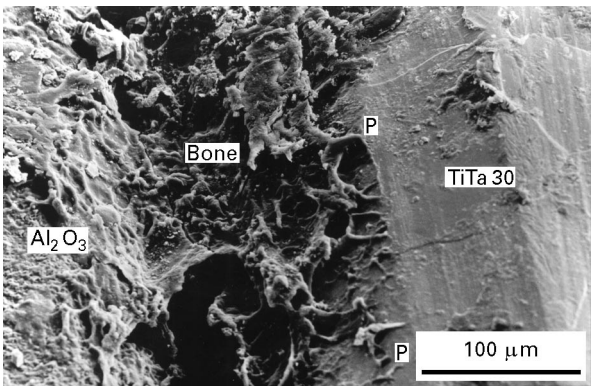

Figure 6 High magnification of the metal–ceramic/bone interface. **P**, contact points.

be an artefact resulting from the dehydration step of the sample preparation. In all cases, the dark interlayer appears to be without any structure. A sharp interface exists between the bright bone and the dark interlayer, **DI**. The chemical composition of the bright bone and the dark interlayer, **DI**, shows differences in both regions. The Ca/P ratio of the bright bone (roughly equal to 1.6) (Fig. 4) is comparable to that of living bone tissue [17, 18]. The Ca/P ratio is dramatically decreased in the dark interlayer, **DI**, while the high C/Ca ratio confirms that the organic component is dominant in this region. The large amount of carbon explains the dark contrast in the scanning electron micrograph because of the low mean atomic weight of the interlayer.

The results of the morphology and the chemical analysis of the implant/bone interface are in agreement with the fracture surface studies performed by SEM and AES. The fracture surface of the composite implant shows a contact between bone and both of the materials (Fig. 5). A good contact to the material is confirmed at higher magnification (Fig. 6). Bonding between implant and bone is achieved by contact points, **P**, in the same way as fibroblasts are attached to microtextured surfaces [19]. The bone tissue adapts to the surface topology especially at the interface region. The presence of tissue at the top of the implant surface implies high fracture toughness of the implant/bone interface.

The chemical composition of the fracture surface of the implant was also analysed by AES. The tissue was found to be mainly organic with small contents of calcium and phosphorus (Fig. 7). Depth profiling of

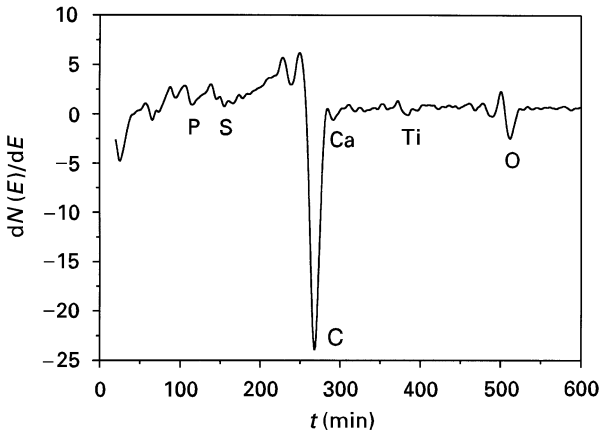

Figure 7 Auger spectrum of the metal side of the implant fracture surface. The surface tissue layer consists mainly of carbon and only of small amounts of calcium and phosphorus.

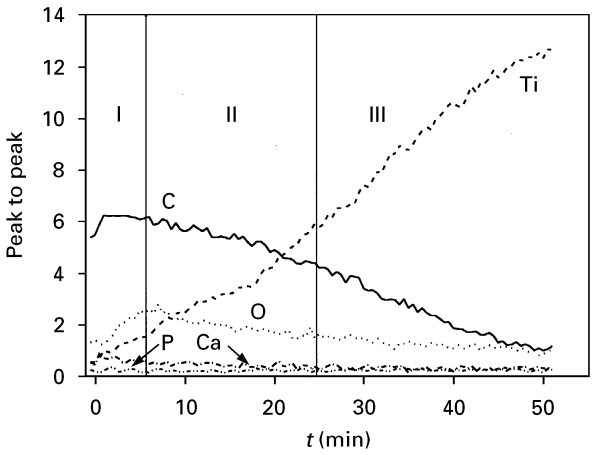

Figure 8 Depth profile of the metal side of the implant surface through the tissue layer of about 730 nm. (I) 2.2 nm min^{-1}, 13.2 nm; (II) 7.7 nm min^{-1}, 138.6 nm; (III) 20 nm min^{-1}, 580 nm.

the surface by sputtering with argon ions indicates a thickness of the tissue layer of about 730 nm (Fig. 8).

3.2. Al_2O_3/bone interface

The interface morphologies described above were also observed for the alumina implant. A cross-section of an alumina implant surrounded by bone observed by SEM is shown in Fig. 9. Dark areas (**D**, **A**) of different dimensions are incorporated within the bright matrix.

A fibrous structure, **C**, surrounding the ellipsoidal dark areas, **A**, is shown in Fig. 10. In some cases, nuclei, **N**, are observed in the dark regions, **A**. The fibres are mainly aligned parallel to the implant surface. Inside the fibre bundles small holes, **OC**, of a diameter of less than 10 μm are observed. A thin gap with bridges, **B**, between material and bone is observed. It cannot be excluded that this gap is, in fact, a crack produced during the preparation process. EDS analysis shows that the dark area, A, is rich in phosphorus and sulphur. A sodium peak is also observed in

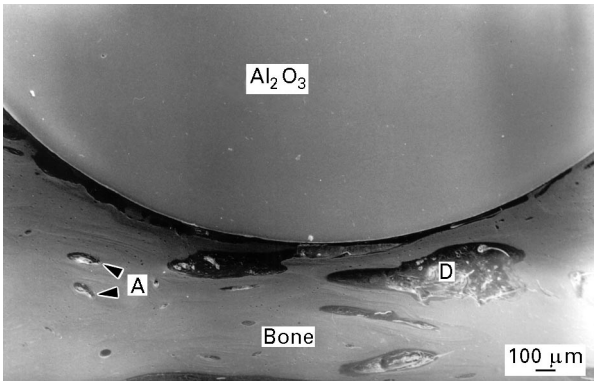

Figure 9 Scanning electron micrograph of Al_2O_3/bone interface.

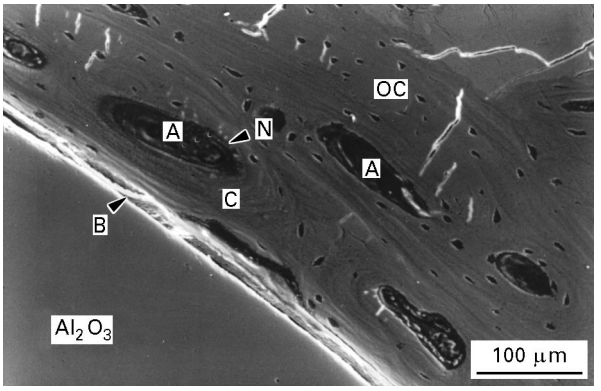

Figure 10 Fibrous structure, **C**, surrounding cell-like dark structures, **A**, near the interface. In the centre of some of these dark areas, a structure that could correspond to a nucleus, **N**, is observed. **B**, brigdes at the interface; **OC**, osteocytes.

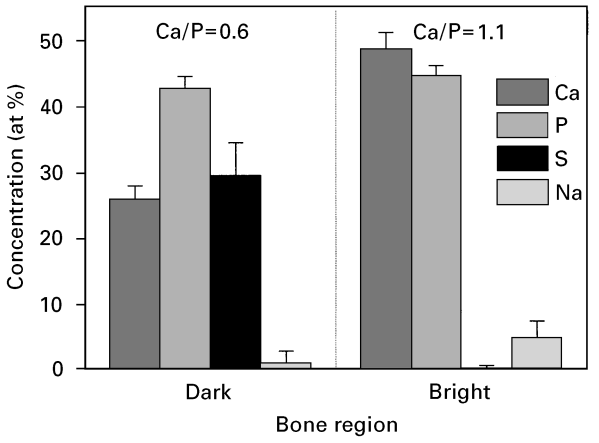

Figure 11 Chemical composition of the bone phases near the Al_2O_3/bone interface.

addition to the calcium and phosphorus peaks in the bright bone phase (Fig. 11).

An interlayer between bone and implant is detected at higher magnification (Fig. 12). It is about 10 μm thick and is interrupted by a lacuna, **L**. Several contact points, **P**, between material and tissue are observed. The interlayer is rich in carbon and contains chemical species from both implant and bone (Fig. 13). The

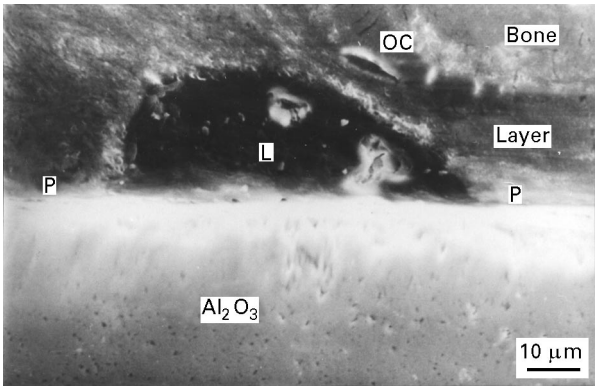

Figure 12 Al_2O_3/bone interface with a thin interlayer of about 10 μm. The interface is interrupted by a lacunae, **L**. **P**, contact points; **OC**, osteocytes.

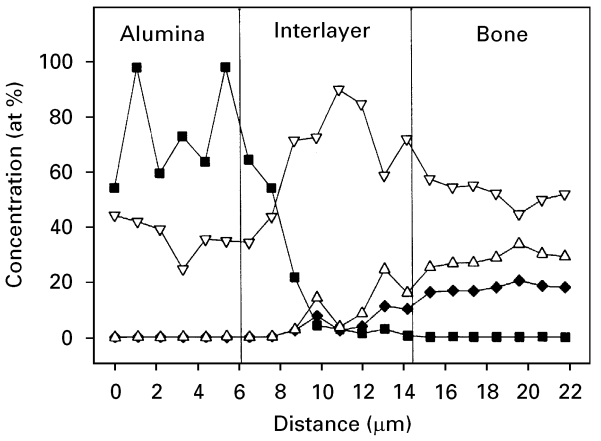

Figure 13 EDS analysis across the Al_2O_3/bone interface layer. (■) Al, (◆) P, (△) Ca, (▽) C.

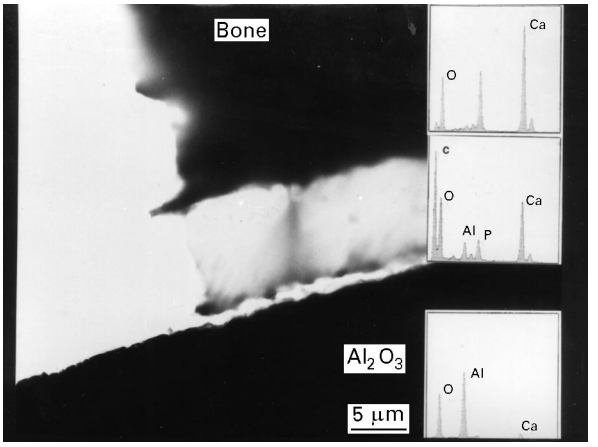

Figure 14 Transmission electron micrograph and EDS point analysis of the Al_2O_3/bone interface.

calcium and phosphorus contents decrease in the direction from bone to alumina, while the aluminium content varies vice versa. The aluminium content decreases with increasing distance to the implant surface. No aluminium is detected away from the interface. Both the interface morphology and the chemical composition of the interlayer are also observed at high magnification by transmission electron microscopy

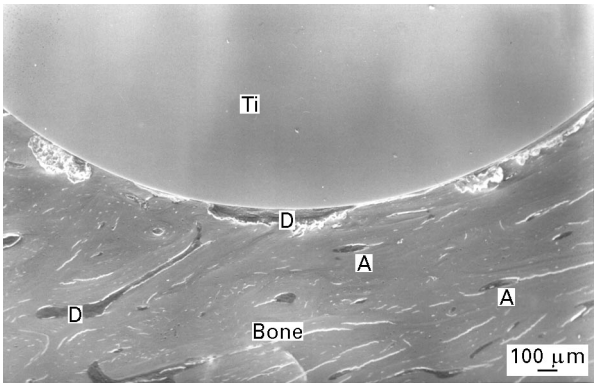

Figure 15 Scanning electron micrograph of a titanium implant/bone interface.

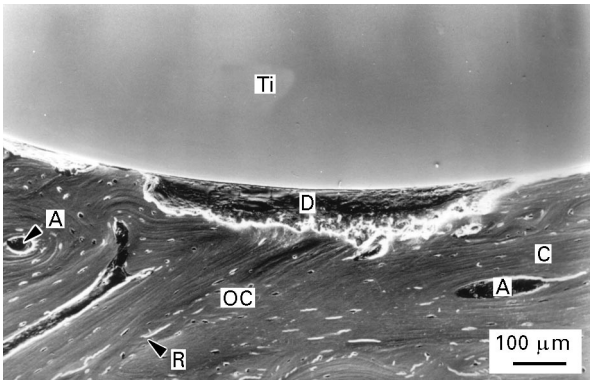

Figure 16 Scanning electron micrograph of the bone tissue surrounding a titanium implant. The bright bone consists of a fibrous structure engulfing ellipsoidal structures, **A**. Blood vessels, **R**, are also visible.

(TEM) (Fig. 14). Bone tissue and alumina are separated by an electron-transparent layer about 15 μm thick. As the sample was not stained, no information concerning the presence of cells and/or proteins was obtained. Chemical analysis shows the presence of aluminium at the interface close to the bone tissue, while this chemical element is not present a few micrometres away in the dark region corresponding to the bone tissue. As expected, both aluminium and oxygen are present in the ceramic, while no aluminium is present in the bone, only the constituents of calcium hydroxyapatite (calcium, phosphorus and oxygen) are found.

3.3. Titanium/bone interface

For the alumina/bone interface, both the interface region and the bone structure close to the implant were studied. A bright bone matrix and a dark second phase are already observed at low magnification (Fig. 15). At a higher magnification, the fibrous structure of the bone matrix engulfing ellipsoidal structures, **A**, is visible as well as small ellipsoidal structures, **OC**, elongated in the direction of the fibres, **C**. The bundles of fibres, **C**, make way for the dark structureless second bone phase, **D**. The bright rod-like structures, **R**, are likely to be blood vessels (Fig. 16). An interlayer is detected at higher

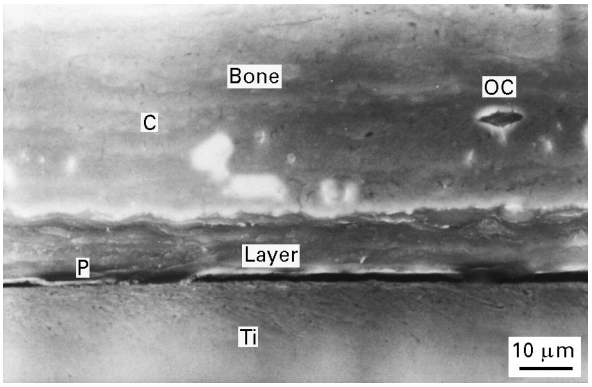

Figure 17 Scanning electron micrograph of the titanium/bone interface with an interfacial layer of a thickness of about 10 μm.

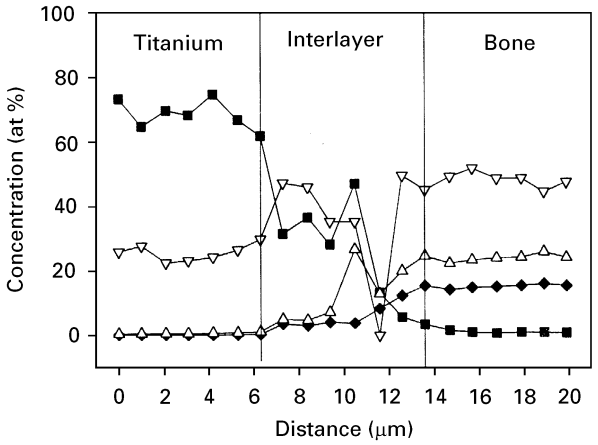

Figure 18 EDS analysis across the interface layer from titanium to bone. The layer is enriched in carbon and consists of species of both implant and bone. (■) Ti, (◆) P, (△) Ca, (▽) C.

magnification (Fig. 17). This layer is about 10 μm thick and is limited by sharp interfaces to both bone and implant. Contacts between bone and material are observed at points, P. The contact area covers about 30% of the interface. This is a result comparable to histomorphometric analysis performed elsewhere [13, 14]. Bright bone phase seems to have a fibrous structure, C; ellipsoidal structures, OC, with a length of less than 10 μm are also visible on the right-hand side of the micrograph. The composition profile across the interface shows that chemical species from both implant and bone coexist in the interlayer (Fig. 18). The calcium and phosphorus contents decrease from the bone to the implant, while the titanium content varies in the opposite direction and is negligible in the bone itself.

4. Discussion

The micrographical and analytical studies performed at the implant/bone interfaces of titanium, Ti–30 wt % Ta and Al_2O_3 show no significant differences in the attachment of bone to the different materials (Table I, Fig. 16) and in the concentration of osteocytes in the bone matrix near the implant surfaces.

The arrangement of cells inside the bone (Figs 1–3) is well-ordered. The osteocytes are included within a flux of collagen fibres surrounding the implant (Fig. 1). This observation is in agreement with histological studies of screw-type titanium implants carried out by optical as well as electron microscopy [20–24]. A comparison of the cell structures seen in Figs 1–3 and 10 with electron microscopical studies of this bone region made by Sennerby *et al.* [24], confirms that the ellipsoidal structures observed are indeed osteocytes bordered by canaliculi. The osteocytes interact directly with the implant by seaming its surface and laying down new bone (Fig. 1). The welding zone between Ti–30 wt % Ta and alumina does not show any negative influence on bone (Fig. 1), hence biocorrosive effects can be excluded at this location.

An intermediate layer was observed at the interface between material and bone. The thickness of this layer was measured by depth profiling to be about 700 nm. According to Tengvall and Lundström [5] and Kasemo and Lausmaa [25], the titanium oxide protecting the implant is not attacked by dissolution. The growth of the oxide layer is supported by proteins adsorbed at the surface. These proteins are products of the cell activity causing an indirect interaction between cells and biomaterial. The mechanisms can also involve the presence of oxygen radicals and peroxy species, generated by cells such as macrophages, that are capable of accelerating the oxidation process [5]. In a physiological environment, an exchange of anions and cations by diffusion leads to an increase of the surface layer. Scanning electron micrographs confirm both the existence of soft tissue bonded to the implant surface by contact points, and the tissue adaption on the implant, independently of the material used. The attachment occurs in the same manner as that of fibroblasts on microtextured titanium surfaces tested *in vitro* [19]. Intact 10 μm thick interface regions are sometimes observed at higher SEM magnifications (Figs 12 and 17). Additionally, gaps and interlayers of a thickness of about 10 μm were observed. However, the gaps shown in Figs 11 and 17 seem to be artefacts produced in the preparation of the explant. They are independent of the materials used. This can be due to the shrinking of the tissue during the preparation process. In some cases, bridges between the implant and bone are observed. The existence of these bridges implies a high bond strength of the bone/implant interface. Poor fitting of the implant can be excluded, because the bone surface seems to replicate the implant surface.

Structures other than osteocytes and collagen fibres were observed. A dark phase with a length of more than 100 μm was found within the bone close to the implant surface as shown on the right-hand side of Fig. 1. Dark phases can also be observed close to the interface and inside the new bone next to the Ti–30 wt % Ta/Al_2O_3 implant (Figs 1 and 2), next to the Al_2O_3 implant (Figs 9 and 10) and next to the titanium implant (Figs 15 and 16). These structures most likely represent the remains of multinuclear giant cells resulting from the inflammation process produced by the implantation of the devices. The

presence of cells near the interface (Figs 10 and 16) or in direct contact with it (Figs 1 and 2) has also been observed by Johannson *et al.* [22]. Furthermore, Sennerby *et al.* [23] report that the dark layer at the implant/bone interface results from tissue formed by multinuclear giant cells. Such cells are more numerous in soft tissue regions where new tissue has not yet grown because of the misfit between the hole drilled in the bone and the implant itself.

The existence of a soft tissue layer close to the implant surface is in agreement with the observations by Sennerby *et al.* [23]. They found that the implant surface is covered by an amorphous layer with a thickness up to 400 nm. The amount of soft tissue decreases with implantation time [9, 26]. Sennerby *et al.* suggest that the tissue close to the implant surface is the last to be mineralized. Dark areas within the bone tissue in Figs 10 and 16 are surrounded by concentric bundles of collagen fibres. These areas are Haversian systems [27, 28].

The chemical composition of the intermediate soft tissue layer is different to that of bone. The high carbon concentration and the small amount of calcium and phosphorus in the dark bone and interface regions (Fig. 4) suggest that soft tissue is mainly composed of organic material. Multinuclear giant cells might be present in the soft tissue. If so, they may play a role in preparing the implant surface for the following formation of new bone [24, 29].

Measurements across the alumina/bone and the titanium/bone interface proved that constituents of the implant (alumina and titanium) and bone are detected in the interlayer. The presence of titanium, calcium and phosphorus inside the interlayer is in agreement with both *in vivo* and *in vitro* studies of titanium implants; see, for example, Li and de Groot [30]. The observed concentration profiles of titanium, calcium and phosphorus are smooth and coexist inside the interlayer. No calcium or phosphorus is found inside the implant and no titanium is detected in the adjacent bone matrix. Studies of the passive dissolution of titanium in physiological environments by AES and EDX confirmed the presence of calcium, phosphorus and sulphur in the oxide surface layer of titanium [31, 32]. The thickness of the oxide layer increases by contact with these organic substances [25, 33].

The mineralization of new bone is shown by an increase of the Ca/P ratio of the matrix [18]. The carbon signal is indicative of the presence of organic material such as collagen. EDS analyses of the soft tissue are confirmed by Auger spectroscopic studies (Figs 7 and 8). The surface of explanted titanium is enriched by carbon, oxygen and small amounts of calcium and phosphorus as observed in other studies [33]. The AES results indicate that a chemical interaction has to exist between the surface of the biomaterial and the living tissue.

Interaction between alumina and bone is demonstrated both by SEM/EDS (Figs 12 and 13) and TEM/EDS (Fig. 14). The gradual transition from the implant to the bone across interlayers with the presence of species of both implant and bone, can enhance the toughness of the implant/bone interface. The detection of aluminium, titanium, calcium or phosphorus inside the interlayer zone is not an artefact, because of the high spatial resolution of the microprobe in respect to the thickness of the interlayer.

5. Conclusion

In the present study, the interfaces formed between bone tissue and three types of material were investigated: Ti–30 wt% Ta/Al_2O_3, Al_2O_3 and titanium implants have been examined by scanning and transmission electron microscopy as well as by EDS analysis. Interfaces showing either a direct implant to bone transition or intermediate layers between the two materials were observed. Interdiffusion of chemical elements from the material (aluminium or titanium) to the bone tissue and from the bone (calcium, phosphorus) towards the material is observed inside the interlayer. This interlayer differs from the bone matrix in structure. Dark areas close to the implant surface have a high carbon content. These dark regions are formed either by multinuclear giant cells, fibrous tissue or Haversian systems. The interface between Ti–30 wt% Ta and alumina seems not to affect bone remodelling or the osteocyte concentration. No osteocytes are detected near the implant surface, which confirms that this region is the last to be mineralized. Irregularities such as gaps between material and bone are assumed to be an artefact due to the preparation process. Some alumina grains are detached from the interface. However, the presence of collagen fibres and the mineralization of new bone resulting from an osteocyte activity close to the implant confirms the biocompatibility of the materials used.

The development of a precise knowledge on the interface phenomena between the bone and different materials used in the fabrication of dental and bone implants, is essential for the understanding of biocompatibility and hence for the design of implants with long-term stability.

Acknowledgements

The authors thank the German Research Community (DFG) for financial support of this work which was performed within the Sonderforschungsbereich 175 'Implantologie' of the DFG centred at the University of Tübingen, Germany. They are greatful to Mrs D. Müller, Mrs K. Zuber and Mr M. Pudleiner for their assistance in the experimental work and specimen preparation. Special thanks are extended to Mrs M. Kaplan for checking the paper from the biological point of view. Professor Dr K. Donath is thanked for making the implant specimens of the Tübingen research group available for this work. Professor E. F. Brès thanks the Alexander von Humbolt Foundation for a fellowship.

References

1. P. TETSCH, "Enossale Implantationen in der Zahnheilkunde" (Hanser Verlag, München-Wien, 1983).

2. T. M. SKERRY, L. BITENSKY, J. CHAYES and L. E. LANYON, *J. Orthop. Res.* **6** (1988) 547.
3. R. A. FULLER and J. J. ROSEN, *Spectrum Wissenschaft* **12** (1986) 86.
4. E. DÖRRE, *Zahnärztliche Praxis* **31** (1980) 343.
5. P. TENGVALL and I. LUNDSTRÖM, *Clin. Mater.* **9** (1992) 115.
6. D. KORN, G. ELSSNER, G. PETZOW and W. SCHULTE, *Z. Zahnärztliche Implantologie* **8** (1992) 136.
7. B. d'HOEDT, A. CHRIST, I. ORTLEPP, K. DONATH, B. GIBBESCH, V. WADEWITZ, G. ELSSNER, J. BREME, G. PETZOW and W. SCHULTE, in "13th Wissenschaftl. Tagung des Arbeitskreises Implantologie innerhalb der DGZMK gem. mit d. Schweiz. Ges. für Orale Implantologie in Zürich" (SGI/SSIO) (1990).
8. B. d'HOEDT, W. SCHULTE, S. HANDTMANN, G. GOMEZ-ROMAN, A. MESCHENMOSER, K. DONATH, I. ORTLEPP, J. BREME, V. BIEHL, G. PETZOW, G. ELSSNER and D. KORN, in "17th Wissenschaftl. Jahrestagung der Arbeitsgemeinschaft Implantologie innerhalb der DGZMK in Mainz" (1994).
9. V. BIEHL, J. BREME, D. KORN, G. ELSSNER, G. PETZOW, W. SCHULTE, B. d'HOEDT and K. DONATH, in "Beiträge zur Elektronenmikroskopischen Direktabbildung und Analyse von Oberflächen," Herbsttagung EDO EMAS in Saarbrücken, edited by U. Ehrenwert, (R. A. Remy, Munster, 1994) BEDO Vol. 27 (1994).
10. G. SOYEZ, D. KORN, G. ELSSNER, M. RÜHLE, G. PETZOW and W. SCHULTE, in Proceedings of the Werkstoffwoche '96, Stuttgart, May 1996, edited by J. Breme (DGM-Informationsgesellschaft, Frankfurt, 1997), Vol. 4, p. 29.
11. K. DONATH, *Der Präparator* **34** (1988) 197.
12. K.DONATH, G. HILLMANN, M. EHRENFELD and D. RIEDGER, *Z. Zahnärztl. Implantologie* **7** (1991) 58.
13. T. FLECHSIG, PhD thesis, University of Göttingen (1991).
14. F. HENNING, PhD thesis, University of Hamburg (1991).
15. A. SRECKER, U. SALZBERGER and J. MAYER, *Prakt. Metallogr.* **30** (1992) 482.
16. D. BRIGGS, M. P. SEAH, "Practical Surface Analysis by Auger and X-Ray Photoelectron Spectroscopy" (Wiley, New York, 1983).
17. M. G. TAYLOR and K SIMKISS, in "Biomineralization Chemical and Biochemical Aspects", edited by S. Mann, J. Webb and R. J. P. Williams (VCH, Weinheim, 1989) p. 427.
18. A. S. POSNER, *Clin. Orthop.* **200** (1985) 87.
19. J. MEYLE, K. GÜLTIG, H. WOLBURG and A. F. VON RECUM, *J. Biomed. Mater. Res.* **27** (1993) 1553.
20. P. THOMSEN and L. E. ERICSON, *Biomaterials* **6** (1985) 421.
21. L. LINDER, K. OBRANT and G. BOIVIN, *Acta Orthop. Scand.* **60** (1989) 135.
22. C. B. JOHANSSON, J. LAUSMAA, T. RÖSTLUND and P. THOMSEN, *J. Mater. Sci. Mater. Med.* **4** (1993) 132.
23. L. SENNERBY, P. THOMSEN and L. E. ERICSON, *ibid.* **4** (1993) 240.
24. *Idem*, *ibid.* **4** (1993) 494.
25. B. KASEMO and J. LAUSMAA, *Mater. Sci. Eng.* **C1** (1994) 115.
26. C. B. JOHANSSON and T. ALBREKTSSON, *Int. J. Oral Maxillofacial Implants* **2** (1987) 69.
27. P. W. FAWCETT, in "Histology" (R. O. Greep, MacGraw-Hill, New York, 1954) p. 132.
28. D. E. STEFLIK, R. V. McKINNEY, A. L. SISK, G. R. PARR and D. L. KOTH, *Scanning Microsc.* **4** (1990) 1021.
29. P. VAN TRAN, A. VIGNERY and R. BARON, *Cell Tissue Res.* **225** (1982) 283.
30. P. LI and K. DE GROOT, *J. Biomed. Mater. Res.* **27** (1993) 1495.
31. K. E. HEALY and P. DUCHEYNE, *ibid.* **26** (1992) 319.
32. K. E. HEALY and P. DUCHEYNE, *J. Mater. Sci. Mater. Med.* **3** (1993) 117.
33. J.-E. SUNDGREN, P. BODÖ and I. LUNDSTRÖM, *J. Coll. Interface Sci.* **110** (1986) 9.

Received 31 October 1996
and accepted 28 January 1997